Methane Emission Management in a Dual-Fuel Engine Exhaust using Pd and Ni Hydroxyapatite Catalysts

Joanna Kamieniak, Peter J. Kelly, Craig E. Banks, Aidan M. Doyle*

Faculty of Science and Engineering, Manchester Metropolitan University, Chester Street, Manchester M1 5GD, UK

* Corresponding author: a.m.doyle@mmu.ac.uk

Abstract

While dual-fuel engines reduce transportation costs and CO_2 emissions by using alternative energy sources e.g. natural gas, the exhaust streams often contain quantities of emissions that exceed limits and therefore require removal. Pd- and Ni-hydroxyapatite (HAP) catalysts were prepared using a soft-templating method and tested in the dry reforming of methane (DRM) in a fixed bed reactor that simulates an exhaust from a diesel-natural gas dual-fuel engine. XRD revealed the characteristic HAP crystal structure of all the prepared materials. The HAP phase was further confirmed by TEM, which also showed the presence of submicron sized particles. The BET surface areas of HAP prepared using a single surfactant was 27.7 m^2g^{-1} and increased to 84.9 m^2g^{-1} when mixed surfactants were used. Active metals were added to HAP using either incipient wetness impregnation, ion-exchange or solid dispersion. All the catalysts tested were active in DRM with the optimal samples converting over 85% of methane at 650 °C.

Keywords: Dry reforming of methane, dual-fuel, hydroxyapatite catalysts

1. **Introduction**

Methane is a major component of natural gas and a widely used fuel source for domestic heating and electricity generation. The process of fracking has allowed previously unrecoverable natural gas reserves to be extracted from shale beds and it is predicted that the USA currently has sufficient natural gas reserves to last at least a century at current usage.[1] Dual-fuel engines provide the opportunity of using alternative energy sources in diesel based compression ignition engines.[2] During dual-fuel operation the engine is fuelled by two fuels simultaneously, whereby combustion of the secondary fuel occurs alongside the conventional compression-induced ignition of diesel.[3] The operating costs of the diesel engine are reduced by adding natural gas in the form of compressed natural gas (CNG) or liquefied natural gas (LNG).[4] While fracking currently allows access to a plentiful supply of CNG, additional renewable pathways exist for natural gas e.g. biomethane, which may in time be a viable substitute for fossil fuels.[5] Dual-fuel operation using CNG produces less CO_2 than the equivalent diesel engine, making such applications highly desirable in the search for decarbonisation of transport systems, but give higher carbon monoxide and hydrocarbon emissions.[6, 7] The main problem relates to the high quantity of methane in the feedstock that produces levels of unburned methane in exhaust gasses that exceed those permitted by current emissions legislation (developed for single fuel engines); the abatement of this methane is the focus of much research.[8, 9] It is possible to decompose methane by an oxidation process using techniques such as steam reforming, partial oxidation, autothermal reforming, and dry reforming of methane (DRM) with carbon dioxide.[10-13] DRM over precious metal heterogeneous catalysts has received much attention and a number of reviews have been published.[14-16]

Calcium hydroxyapatite (HAP), $Ca_{10}(PO_4)_6(OH)_2$, has an elemental composition similar to that found in teeth and bones, and has been used as a substitute material in dental and orthopaedic medical fields.[17] HAP possesses a characteristic hexagonal structure of PO_4 tetrahedrons, with the $P6_3/m$ space group, whereby charge-balancing Ca^{2+} and OH^- ions reside on the c-axis.[18] Their high structural stability, bifunctionality of acidic and basic sites, and the possibility of isomorphous substitution mean that HAPs are excellent catalyst supports, as summarised in a recent review.[19] Their hydrophilic properties allow them to be used directly as heterogeneous catalysts in dehydration reactions *e.g.* reaction of lactic acid to produce acrylic acid, an important intermediate for acrylate polymers and other key molecules,[20, 21] and also in the Guerbet coupling of alcohols.[22-24] The addition of

metals, either as nanoparticles and/or substituted into the framework, greatly increases the range of reported reactions to include; acetone condensation,[25] water-gas shift,[26] alkane dehydrogenation/oxidative coupling,[27-31] alcohol synthesis/transformation[32, 33] and the oxidation of (a) volatile organic compounds[34-36] (b) alcohol[37,38] (c) carbon monoxide[39] and (d) methane[40-42]. Ni loaded HAP has been reported to be active in DRM with 100% methane conversion at approximately 700 °C.[43] Yoon and co-workers studied the effects of adding cerium to Ni/HAP catalysts with a view to reducing the well-established tendency for Ni to generate carbon deposits during reaction. Results showed that temperatures in excess of 700 °C were required for >90% conversion and that cerium doped samples enhanced the catalytic stability due to the oxygen storage capacity of ceria preventing excessive carbon deposition.[44]

In this paper we report the successful preparation of Pd- and Ni-HAP catalysts using a soft-templating synthesis route. Our results confirm that these materials are active catalysts in the DRM reaction. To our knowledge, this is the first report of DRM over a Pd-HAP heterogeneous catalyst.

2. Experimental

2.1 Materials and chemicals

All chemicals; calcium nitrate tetrahydrate (>99%), potassium phosphate monobasic (>99%), ammonia solution 25% (v/v), polyoxyethylene(20) sorbitan monostearate (10% in H_2O), nonaoxyethylene dodecyl ether, nitric acid 70% (v/v), ethanol (98%), palladium nitrate dehydrate (40% of Pd content), palladium chloride (99%), nickel nitrate hexahydrate (>98.5%) and nickel oxide (99%) were obtained from Sigma-Aldrich, Dorset, UK and used as received without any further purification. All solutions were made using deionised water with resistivity not less than 18.2 MΩ cm.

2.2 Catalyst synthesis

Hydroxyapatite (HAP) synthesis was based on a method reported elsewhere.[45] $Ca(NO_3)_2$ (7.88 g) was mixed with KH_2PO_4 (2.72 g), dissolved in deionised water (26.60 mL) and acidified by concentrated HNO_3 (13.60 mL) to avoid precipitation of $Ca_2(PO_4)_3$. This acidic solution was then added to a mixture of either polyoxyethylene(20) sorbitan monostearate (Tween 60, 26 g), or Tween 60 and nonaoxyethylene dodecyl ether ($C_{12}EO_9$, 26 g and 10.66 g, respectively) and heated to 60 °C with stirring until a clear solution was formed. The

solution was cooled to room temperature and treated with NH_3 (44.0 mL) added dropwise to precipitate HAP. The suspension was stirred overnight, filtered, washed with ethanol and water, dried and calcined in air for 5 hours at 550 °C.

For ion exchanged catalysts, 50 mg of metal salt ($PdCl_2$, $Pd(NO_3)_2$ or $Ni(NO_3)_2$) was dissolved in 100 mL deionised water (dispersed in the case of NiO), added to 1 g HAP and the resulting mixture stirred for three days at room temperature, filtered, vacuum dried and calcined at 550 °C for 3 hours. For incipient wetness impregnation, 50 mg of metal salt was dissolved in a minimal amount of deionised water and dripped onto 1 g of calcined HAP, mixed, filtered, vacuum dried and calcined at 550 °C for 3 hours. Table 1 summarises all synthetic routes of the catalysts prepared.

2.3 Characterisation

X-Ray diffraction (XRD) was conducted in powder spinning mode at ambient conditions using a Panalytical X'Pert Powder diffractometer with Cu K_α radiation (λ = 1.5406 Å). All powder diffraction patterns were recorded with step size 0.052° and step time 200 s, using an X-ray tube operated at 40 kV and 30 mA with fixed 1/2° anti-scatter slit. XRD patterns for HAP 1 and HAP 2 were taken before catalyst testing while all Ni- and Pd-HAPs were analysed after reaction due to the low quantities available. Nitrogen adsorption/desorption measurements were carried out using a Micromeritics ASAP 2020 Surface Analyser at -196 °C. Samples were degassed under vacuum ($p < 10^{-5}$ mbar) for 3 h at 300 °C prior to analysis. BET surface areas of the samples were calculated in the relative pressure range 0.05-0.30. Microscopic images were recorded using a Supra 40VP (Carl Zeiss Ltd, UK) scanning electron microscope (SEM) or JEOL JEM 210 transmission electron microscopy (TEM). Semi-quantitative chemical analysis was performed by energy-dispersive X-ray spectroscopy (EDAX) using an Apollo 40 SDD instrument. Thermogravimetric analysis (TGA) measurements were recorded using a Perkin Elmer 4000 instrument heated at 10 °C min^{-1} from 25-820 °C in 40.0 mL min^{-1} flowing air or nitrogen.

2.4 Catalytic tests

The catalyst activity of each sample was studied in a quartz fixed bed reactor, Figure 1, placed inside a temperature controlled furnace (Carbolite type 3216, Tempatron, PID500/110/330). A sample of catalyst (0.2 g) catalyst was placed in a quartz tube (10 mm diameter, 1 mm thickness) between quartz wool plugs. A feed mixture of 100 mL min^{-1}

comprising CH_4:CO_2:He equal to 5:5:90 was used in all catalytic tests. Gases were supplied from lecture bottles (CKGAS filled to 200 Bar at 15 °C) and regulated using single stage CONCOA 302 series gas regulators. The flow of each gas was maintained using Bronkhorst UK model F-201CV mass flow controllers. Prior to reaction the catalyst was reduced in 30 mL min^{-1} H_2 for 1 hour at 300 °C. The reaction products were monitored by a Hewlett Packard 5890 series II gas chromatograph equipped with a GS-GASPRO column (60 m x 0.32 mm) connected *via* a 6-way gas sampling valve to a thermal conductivity detector. Measurements were recorded at 50 °C intervals (after holding at that temperature for 5 mins) between 205 and 650 °C using a heating rate of 10 °C min^{-1}. The determination of methane conversions was calculated as follows:

$$\mathrm{CH_4\ conversion\ (\%)} = \frac{(\mathrm{CH_4})_{in} - (\mathrm{CH_4})_{out}}{(\mathrm{CH_4})_{in}} \times 100$$

3. Results and Discussion

3.1. Synthesis and characterisation

XRD patterns are shown in Figures 2 and 3, grouped based on metal added, Pd and Ni respectively. HAP 1 and HAP 2 are shown for comparison only *e.g.* Ni catalysts were prepared on both HAP 1 and HAP 2 (see Experimental section 2.2). All samples show the characteristic peaks corresponding to the $P6_3/m$ hexagonal arrangement of HAP and conform to the HAP standard pattern (JCPDS pattern 01-072-1243). The patterns for the catalysts confirm that the crystallinity is preserved after the DRM reaction up to 650 °C. Pd and Ni are also proven to be present in their metallic forms as evidenced by their characteristic reflections in Figures 2 and 3. The mean metal particle sizes were calculated using the Scherrer equation and the results are presented in Table 1. For Cat 2 to Cat 9 the particle size varied in the range 16.1-34.7 nm. The particle size of Pd in Cat 1 was too low to be accurately distinguished from the underlying HAP support due to signal overlap. The Ni particles in Cat 10 are significantly larger than those of the other catalysts, with average dimension 296 nm; this difference is due to its preparation using an insoluble salt, nickel oxide, which is dispersed as a solid over the HAP support as opposed to being precipitated/exchanged from solution as in the other samples. XRD peaks for phases other than HAP, Pd or Ni were also detected for some of the catalysts. For example, Cat 10 shows 2 such peaks that are identified by the symbol ▲ in Figure 3. There is insufficient data here to assign these peaks definitively. However, while the presence of these peaks is obviously

due to impurities, the signals are relatively weak so the impurities constitute a minor part of the sample. SEM images, Figures 4A and 4B, show the agglomerated and crystalline nature of sub-micron sized HAP particles. Such morphology remained practically the same after addition of Pd on the HAP surface (Figures 4C and 4D). TEM analysis of HAP 2, Figure 5A, confirms that there are also irregularly sized porous particles present with dimension <100 nm, while the regular structure of HAP can be clearly seen in Figure 5B as described by Opre *et.al*.[37]

Each catalyst was examined for semi-quantitative metal content using EDAX at three different areas, which provides an estimate of the metal distribution from the % relative standard deviation (%RSD) values. Table 1 summarises these data, together with metal loading approach and BET surface area of each sample. The surface area of HAP 1, which was synthesised using one surfactant (Tween 60), is 27.7 m^2g^{-1} and increases significantly to 84.9 m^2g^{-1} when using mixed surfactants (Tween 60 and $C_{12}EO_9$). Overall, the addition of metals to both HAP 1 and HAP 2 caused variations in surface area. The surface areas for catalysts prepared using the HAP 1 single surfactant method showed a minimum value <1 m^2g^{-1} for Cat 8 and maximum of 45.6 m^2g^{-1} for Cat 1. The surface areas for catalysts prepared using the mixed surfactant method were all lower than that for the HAP 2 support (84.9 m^2 g^{-1}) where the values alternated from 14.4 m^2 g^{-1} for Cat 6 to 46.2 m^2g^{-1} for Cat 3 suggesting the addition of metals caused partial pore blockage. It is important to note, that all Pd- based samples exhibited higher surface areas than Ni-based.

3.2. Catalytic activity.

The catalysts were investigated in the DRM reaction. All catalysts were found to be active as evidenced by the % conversion of methane as a function of temperature shown in Figure 6. There was no significant reaction detected at temperatures below 450 °C, and thereafter the methane conversion increased with temperature. The relative catalyst activities may be assessed by comparing their maximum conversions, which occurred in all samples at the maximum temperature 650 °C. These values for Pd modified HAP were 43% for Cat 1, 57% for Cat 2, 62% for Cat 5, and the most active catalyst was Cat 3, which converted 88% of the methane feed. Ni modified HAP had corresponding values of 31% for Cat 6, 57% for Cat 8, 72% for Cat 9 and a maximum activity of 87% for Cat 10. It is interesting to note that for both metals the highest activity was shown by the catalysts with the highest surface area (46.2 m^2g^{-1} for Cat 3 and 19.8 m^2g^{-1} for Cat 10). Boukha *et al.* also investigated methane reforming over Ni-HAP catalysts but with lower reactant flow rates and catalyst mass (CH_4/CO_2/He =

2/2/60, 0.1 g) than those reported here (CH_4/CO_2/He = 5/5/90, 0.2 g).[43] While the different experimental conditions make it difficult to make an exact comparison between both studies it is remarkable that the conversions observed are broadly similar; Cat 10 decomposes 87 % of methane at 650 °C versus 85-96% conversion at the same temperature for the range of catalysts reported by Boukha. Our results are also broadly similar to those reported by Yoon and co-workers who studied different feed compositions over 0.2 g catalyst.[44] Approximately 77% methane was decomposed in a feed stream comprising CH_4/CO_2/He = 10/10/80 at 650 °C; this is less than observed for Cat 10 (87%). Furthermore, the relatively high conversion of Cat 10 is interesting in that the catalyst was prepared by stirring the HAP in a dispersion of an insoluble salt. This is not the conventional method of catalyst preparation but, nonetheless, the results using the experimental conditions here confirm the activity and stability of this catalyst in DRM. To our knowledge, there are no previous reports showing the reforming of methane with CO_2 using Pd-apatite catalysts. Numerous studies have shown that Pd based catalysts show similar activity but superior stability to that of Ni based catalysts.[14-16] Based on this, the Pd-HAP samples presented here will be tested in a follow-on study to assess their stability in the CO_2 reforming of methane.

3.3 TGA

TGA was performed to test for the presence of coke on the surface of each sample after reaction. The coking process plays a major role in the initial deactivation of the catalysts by covering the catalytically active metal surface.[46] It is possible to estimate the quantity of coke using TGA, as heating in air causes its combustion at temperatures approximately 450 °C and above. However, the active metal and underlying HAP support also undergo reactions when heated, namely oxidation to metal oxide and dehydroxylation, respectively. TGA of Cat 10 in N_2, Figure 7, prevents both Ni oxidation (mass increase) and coke combustion (mass decrease) so this can be used to measure the mass of water lost to HAP dehydroxylation; for Cat 10 this is approximately 5 wt% over the full temperature range. TGA of Cat 10 in air shows a pronounced increase in mass from 400-700 °C, confirming that the mass of oxygen gained by the Ni is greater than the sum of that consumed by the coke and the mass of water lost to dehydroxylation. Overall, this is consistent with Cat 10 containing a minimal amount of coke, which matches well with Cat 10 having the highest recorded activity in the DRM reaction (Figure 6). Similar increases in mass during TGA, and relatively high activity in DRM, are also observed in Cat 2, Cat 3, and Cat 9; these samples also showed lower overall

mass losses than the remaining samples and were among the more active catalysts. Overall, the low mass loss (approximately 5 wt% of which is due to HAP) suggests resistance of the materials to coke formation under the conditions studied here.

4. Conclusions

The methane emissions in a simulated diesel-natural gas dual-fuel engine exhaust were reduced by up to 88% using heterogeneous catalytic DRM. A range of Ni and novel Pd catalysts were prepared over hydroxyapatite (HAP) supports using both ion exchange and incipient wetness impregnation. XRD and TEM confirmed the characteristic crystal structure of HAP. These materials were active heterogeneous catalysts in DRM reaching maximum methane conversions of 87% for Ni-HAP and 88% for Pd-HAP at an operating temperature of 650 °C. This is the first reported example of Pd-HAP catalysing the CO_2 reforming of methane.

Acknowledgements

The authors are grateful to G-volution plc. for their support and contribution to this research.

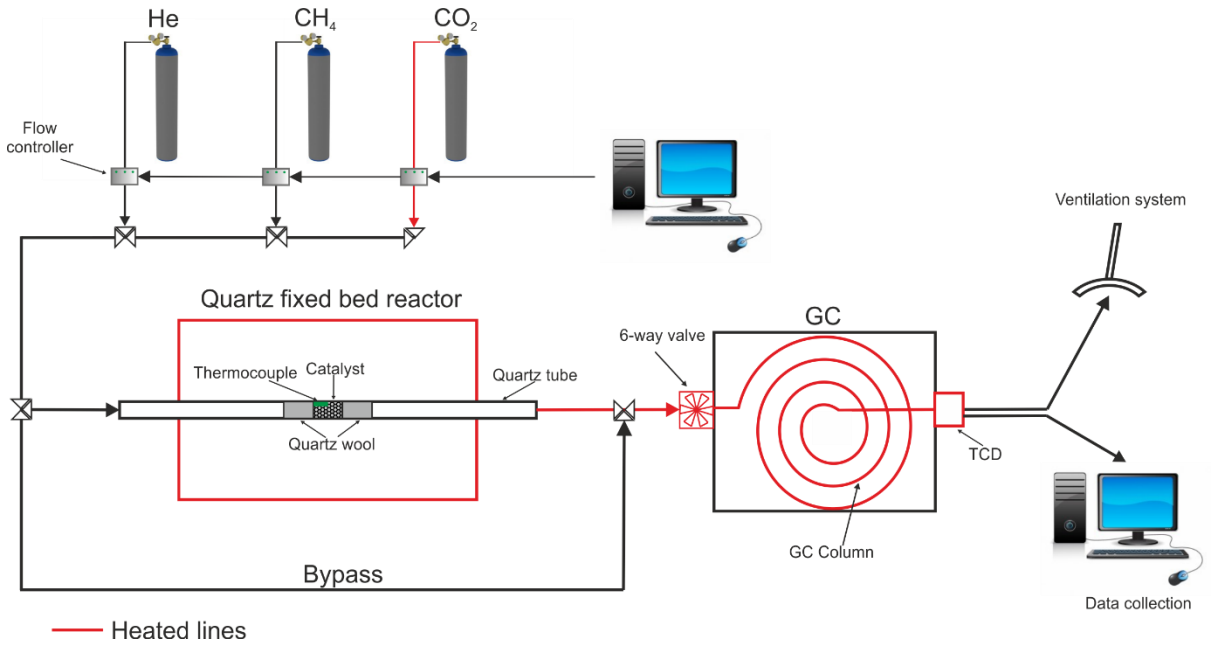

Figure 1. Schematic representation of plug-flow catalyst testing reactor.

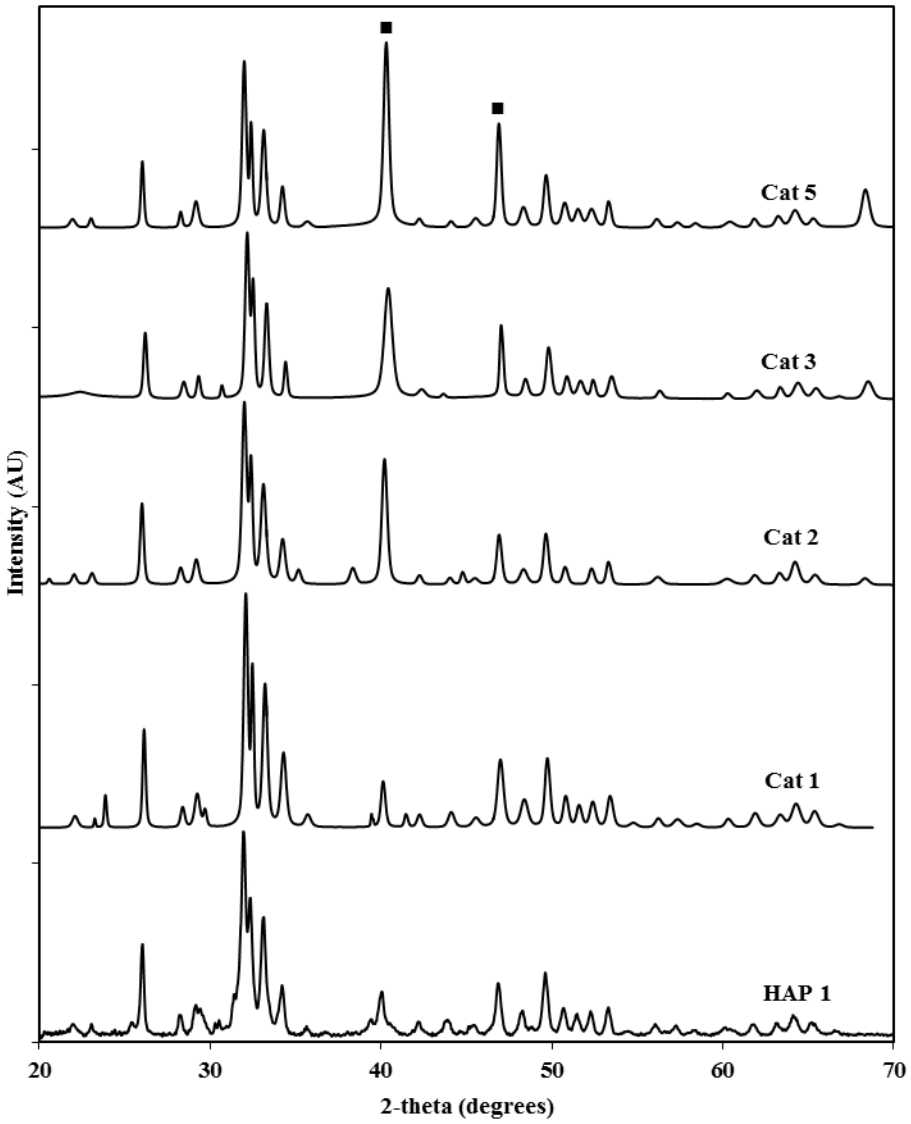

Figure 2. XRD powder patterns of HAP 1 and Pd-HAP catalysts, ■ Pd.

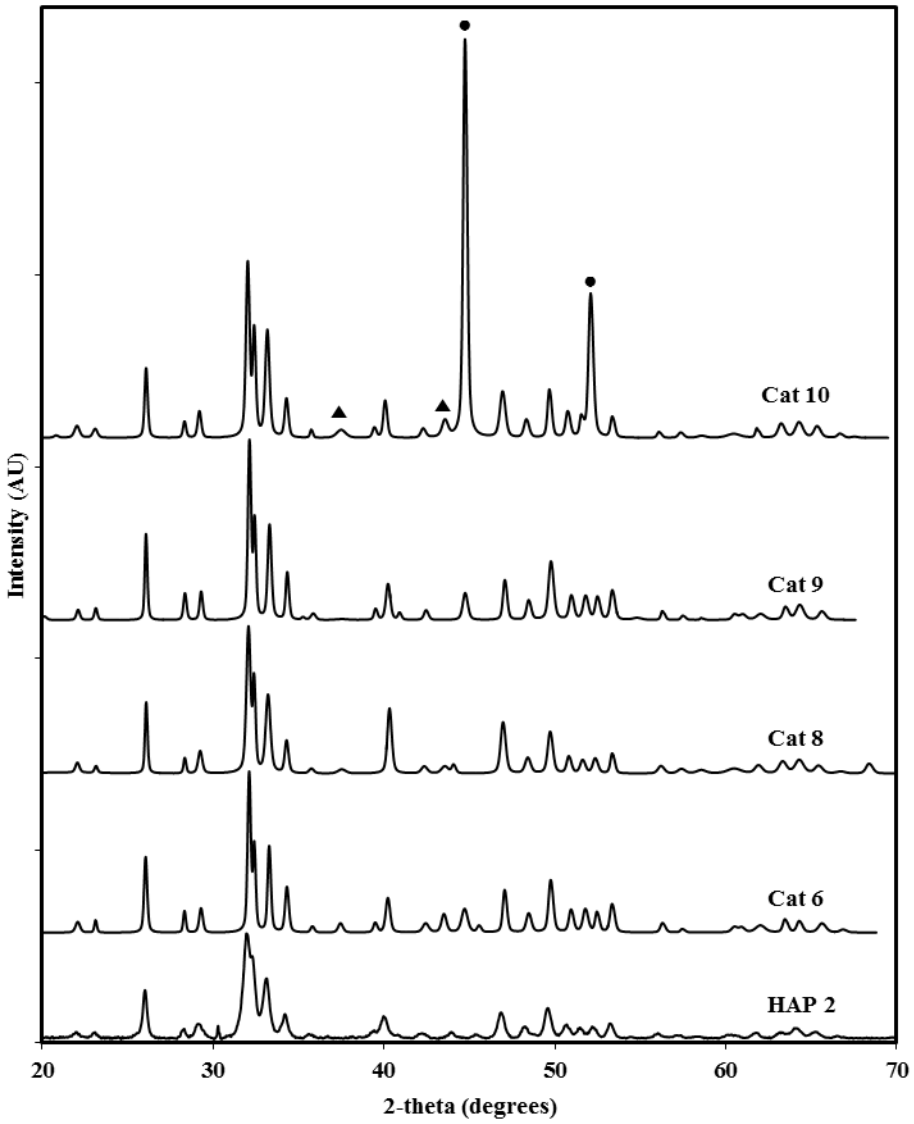

Figure 3. XRD powder patterns of HAP 2 and Ni-HAP catalysts, ● Ni, ▲non-HAP/Pd/Ni phase.

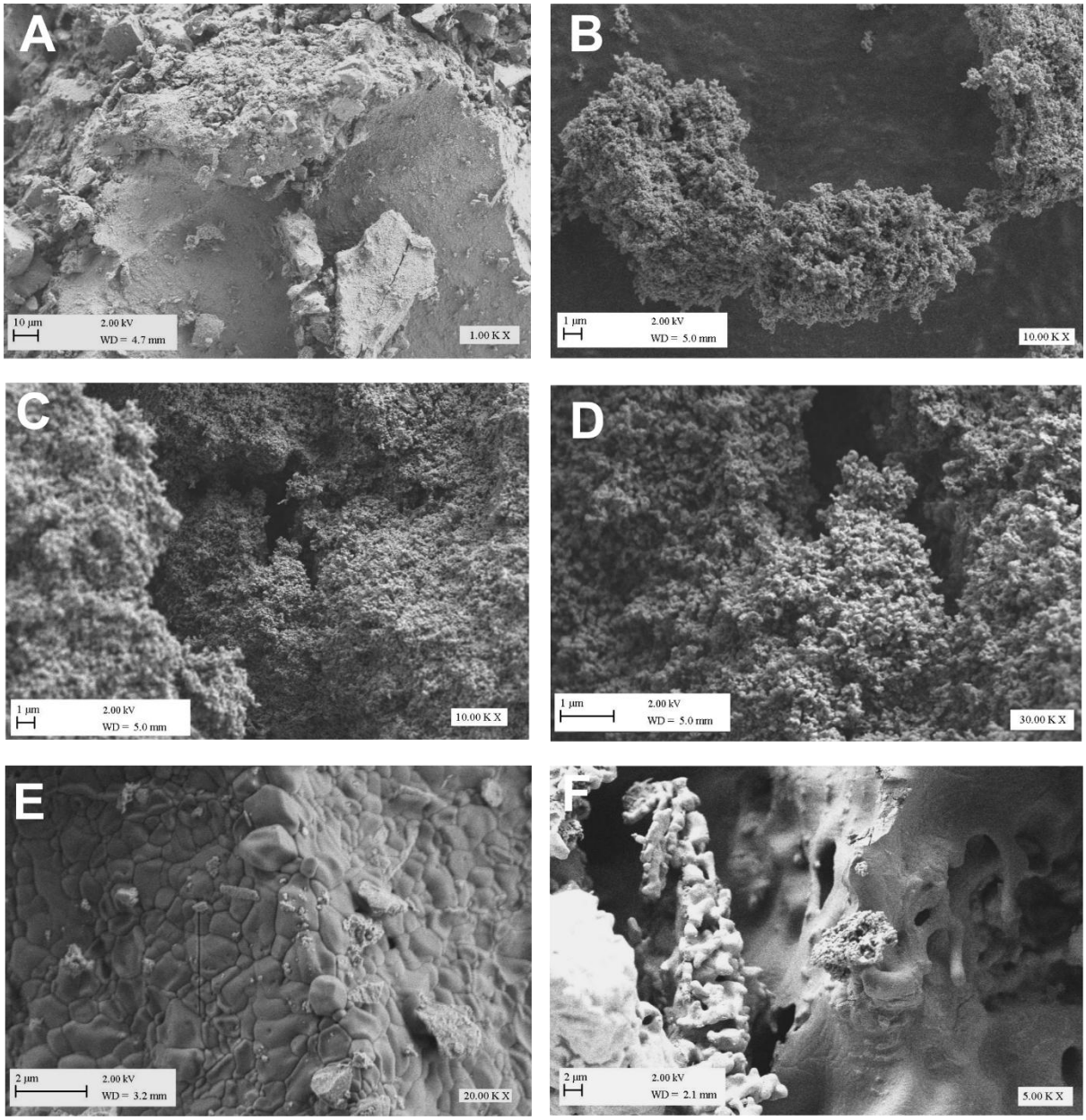

Figure 4. SEM images HAP 1 (A, B), Cat 3 (C, D) and Cat 10 (E, F).

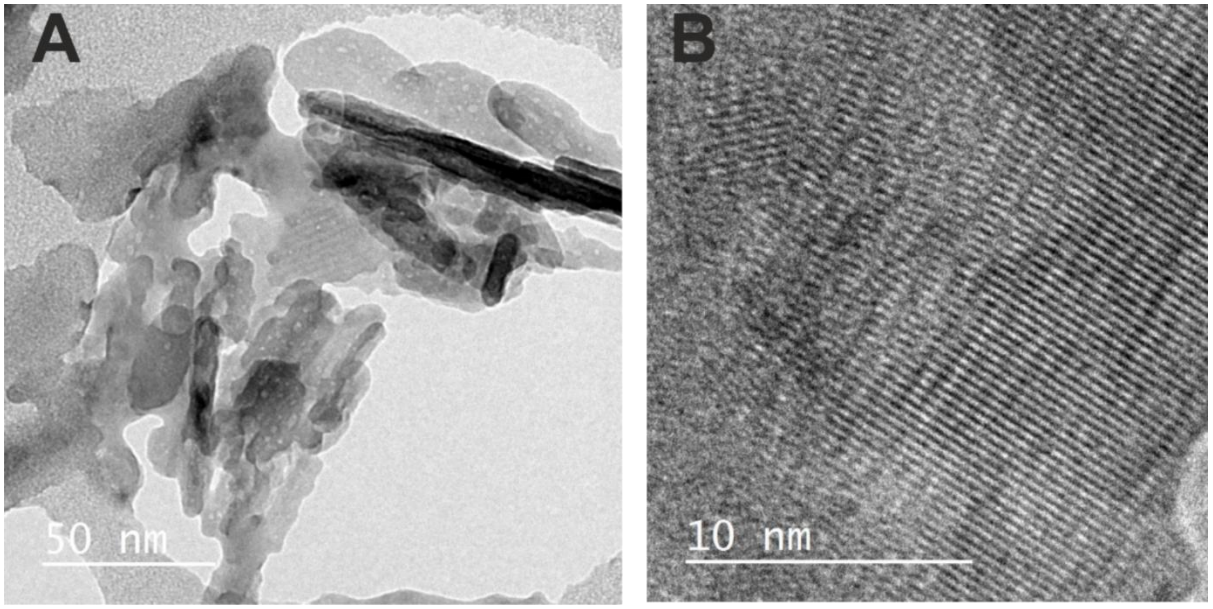

Figure 5. TEM images for HAP 2.

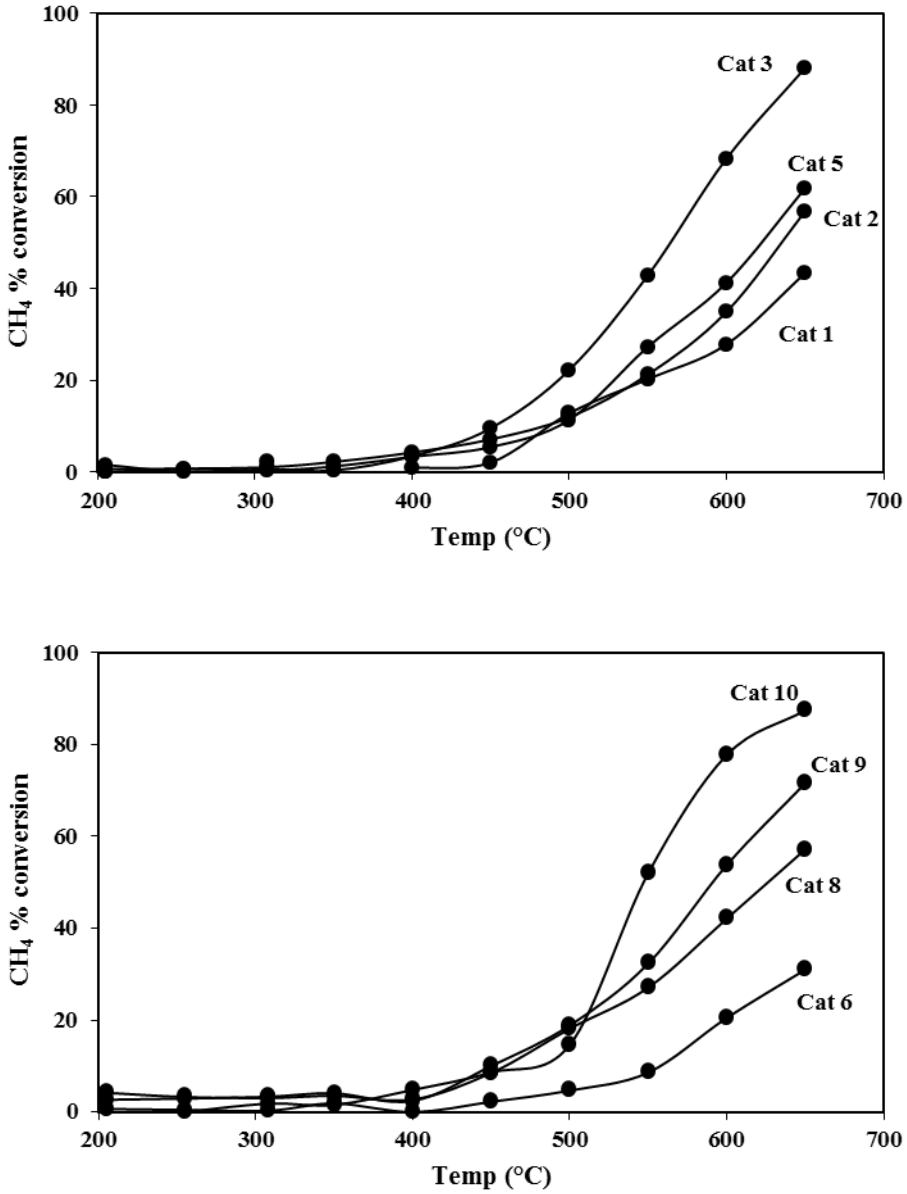

Figure 6. CH_4 conversion over Pd- (top) and Ni- (bottom) HAP as a function of reaction temperature.

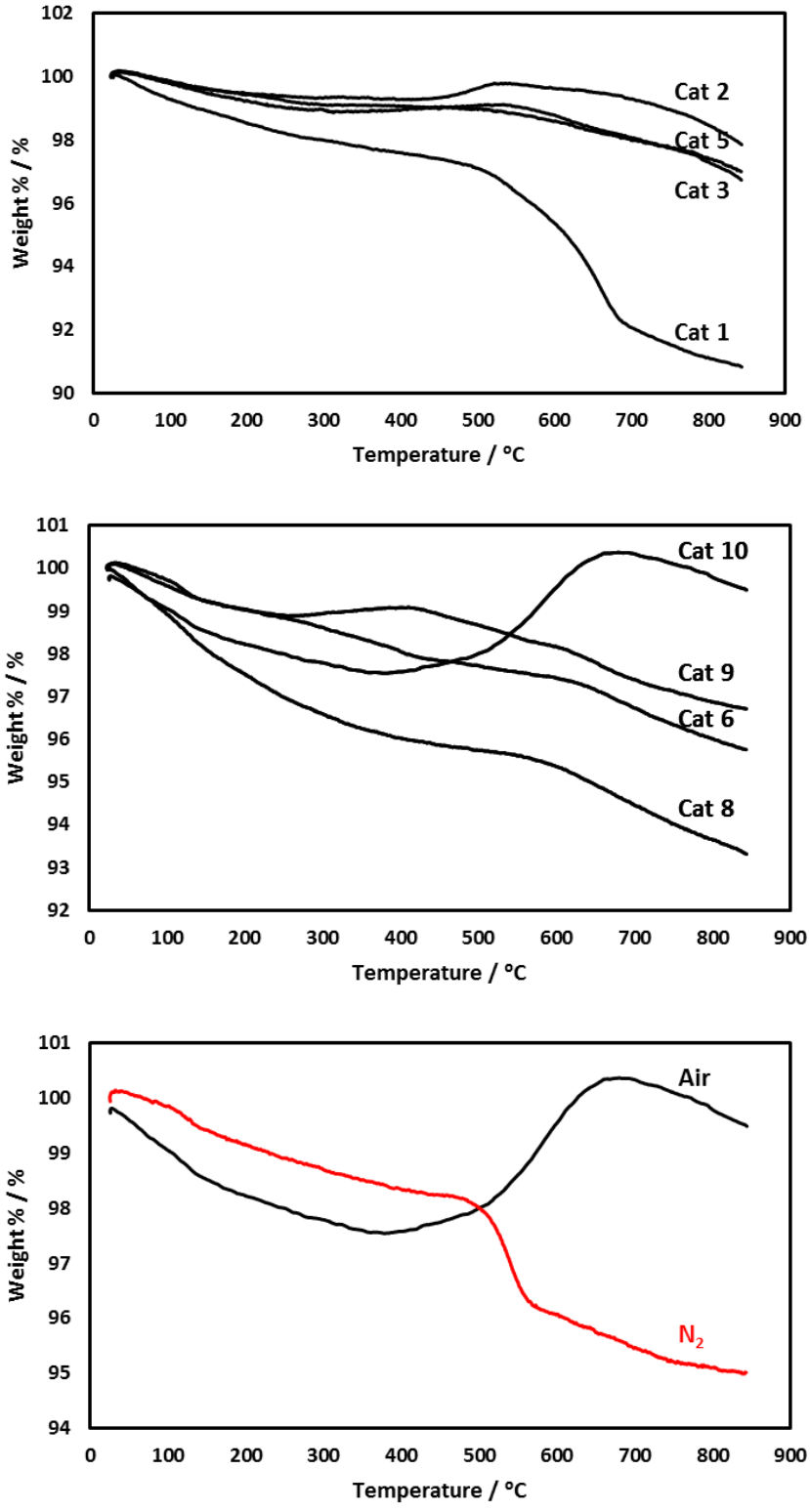

Figure 7. TGA profiles of Pd- based samples in air (top), Ni-based samples in air (middle) and Cat 10 in air and N_2 (bottom).

Table 1: Preparation methods, metal loadings and surface areas. [a]IW incipient wetness impregnation, IE ion exchange; [b]relative standard deviation.

Sample	Surfactant/support used	Metal salt, loading method[a]	Metal loading (wt%)	RSD (%)[b]	Surface area (m^2 g^{-1})	Mean metal particle size (nm)
HAP 1	Tween 60	-	-	-	27.7	
HAP 2	Tween60 + $C_{12}EO_9$	-	-	-	84.9	
Cat 1	HAP 1	$Pd(NO_3)_2$, IW	4.7	12.7	45.6	-
Cat 2	HAP 2	$Pd(NO_3)_2$, IE	13.2	2.5	34.6	18.3
Cat 3	HAP 2	$Pd(NO_3)_2$, IW	13.8	17.8	46.2	16.1
Cat 5	HAP 1	$Pd(NO_3)_2$, IE	4.6	5.6	34.6	30.4
Cat 6	HAP 2	$Ni(NO_3)_2$, IW	15.3	4.0	14.4	25.0
Cat 8	HAP 1	$Ni(NO_3)_2$,IE	9.4	39.4	<1	34.7
Cat 9	HAP 2	$Ni(NO_3)_2$, IE	35.1	19.3	16.5	20.4
Cat 10	HAP 1	NiO	6.0	27.5	19.8	296

References:

[1] U. Izquierdo, V.L. Barrio, J. Requies, J.F. Cambra, M.B. Güemez, P.L. Arias, Tri-reforming: A new biogas process for synthesis gas and hydrogen production, International Journal of Hydrogen Energy, 38 (2013) 7623-7631.

[2] C. Abagnale, M.C. Cameretti, L. De Simio, M. Gambino, S. Iannaccone, R. Tuccillo, Numerical simulation and experimental test of dual fuel operated diesel engines, Applied Thermal Engineering, 65 (2014) 403-417.

[3] J. Benajes, A. García, J. Monsalve-Serrano, I. Balloul, G. Pradel, An assessment of the dual-mode reactivity controlled compression ignition/conventional diesel combustion capabilities in a EURO VI medium-duty diesel engine fueled with an intermediate ethanol-gasoline blend and biodiesel, Energy Conversion and Management, 123 (2016) 381-391.

[4] J. Klimstra, 11 - Fuel flexibility with dual-fuel engines A2 - Oakey, John, in: Fuel Flexible Energy Generation, Woodhead Publishing, Boston, 2016, pp. 293-304.

[5] X. Shan, Y. Qian, L. Zhu, X. Lu, Effects of EGR rate and hydrogen/carbon monoxide ratio on combustion and emission characteristics of biogas/diesel dual fuel combustion engine, Fuel, 181 (2016) 1050-1057.

[6] B. Bharathiraja, T. Sudharsanaa, A. Bharghavi, J. Jayamuthunagai, R. Praveenkumar, Biohydrogen and Biogas – An overview on feedstocks and enhancement process, Fuel, 185 (2016) 810-828.

[7] M. Crippa, G. Janssens-Maenhout, D. Guizzardi, S. Galmarini, EU effect: Exporting emission standards for vehicles through the global market economy, Journal of Environmental Management, 183, Part 3 (2016) 959-971.

[8] Y. Karagöz, T. Sandalcı, U.O. Koylu, A.S. Dalkılıç, S. Wongwises, Effect of the use of natural gas–diesel fuel mixture on performance, emissions, and combustion characteristics of a compression ignition engine Advances in Mechanical Engineering 8(2016) 1-13.

[9] B. Challen, R. Baranescu, Diesel Engine Reference Book, Society of Automotive Engineers, 1999.

[10] R. Horn, R. Schlögl, Methane Activation by Heterogeneous Catalysis, Catalysis Letters, 145 (2015) 23-39.

[11] B. Christian Enger, R. Lødeng, A. Holmen, A review of catalytic partial oxidation of methane to synthesis gas with emphasis on reaction mechanisms over transition metal catalysts, Applied Catalysis A: General, 346 (2008) 1-27.

[12] P. Gélin, M. Primet, Complete oxidation of methane at low temperature over noble metal based catalysts: a review, Applied Catalysis B: Environmental, 39 (2002) 1-37.

[13] J.H. Lunsford, Catalytic conversion of methane to more useful chemicals and fuels: a challenge for the 21st century, Catalysis Today, 63 (2000) 165-174.

[14] D. Pakhare, J. Spivey, A review of dry (CO2) reforming of methane over noble metal catalysts, Chemical Society Reviews, 43 (2014) 7813-7837.

[15] J.-M. Lavoie, Review on dry reforming of methane, a potentially more environmentally-friendly approach to the increasing natural gas exploitation, Frontiers in Chemistry, 2 (2014).

[16] M. Usman, W.M.A. Wan Daud, H.F. Abbas, Dry reforming of methane: Influence of process parameters—A review, Renewable and Sustainable Energy Reviews, 45 (2015) 710-744.

[17] Y.-H. Yang, C.-H. Liu, Y.-H. Liang, F.-H. Lin, K.C.W. Wu, Hollow mesoporous hydroxyapatite nanoparticles (hmHANPs) with enhanced drug loading and pH-responsive release properties for intracellular drug delivery, Journal of Materials Chemistry B, 1 (2013) 2447-2450.

[18] J.M. Hughes, Structure and Chemistry of the Apatites and Other Calcium Orthophosphates By J. C. Elliot (The London Hospital Medical College). Elsevier: Amsterdam. 1994. xii + 389 pp. ISBN 0-444-81582-1, Journal of the American Chemical Society, 118 (1996) 3072-3072.

[19] M. Gruselle, Apatites: A new family of catalysts in organic synthesis, Journal of Organometallic Chemistry, 793 (2015) 93-101.

[20] B. Yan, L.-Z. Tao, Y. Liang, B.-Q. Xu, Sustainable Production of Acrylic Acid: Catalytic Performance of Hydroxyapatites for Gas-Phase Dehydration of Lactic Acid, ACS Catalysis, 4 (2014) 1931-1943.
[21] V.C. Ghantani, S.T. Lomate, M.K. Dongare, S.B. Umbarkar, Catalytic dehydration of lactic acid to acrylic acid using calcium hydroxyapatite catalysts, Green Chemistry, 15 (2013) 1211-1217.
[22] J.T. Kozlowski, R.J. Davis, Heterogeneous Catalysts for the Guerbet Coupling of Alcohols, ACS Catalysis, 3 (2013) 1588-1600.
[23] L. Silvester, J.-F. Lamonier, J. Faye, M. Capron, R.-N. Vannier, C. Lamonier, J.-L. Dubois, J.-L. Couturier, C. Calais, F. Dumeignil, Reactivity of ethanol over hydroxyapatite-based Ca-enriched catalysts with various carbonate contents, Catalysis Science & Technology, 5 (2015) 2994-3006.
[24] T. Tsuchida, T. Yoshioka, S. Sakuma, T. Takeguchi, W. Ueda, Synthesis of Biogasoline from Ethanol over Hydroxyapatite Catalyst, Industrial & Engineering Chemistry Research, 47 (2008) 1443-1452.
[25] N. Cheikhi, M. Kacimi, M. Rouimi, M. Ziyad, L.F. Liotta, G. Pantaleo, G. Deganello, Direct synthesis of methyl isobutyl ketone in gas-phase reaction over palladium-loaded hydroxyapatite, Journal of Catalysis, 232 (2005) 257-267.
[26] D. Miao, A. Goldbach, H. Xu, Platinum/Apatite Water-Gas Shift Catalysts, ACS Catalysis, 6 (2016) 775-783.
[27] S. Sugiyama, T. Minami, H. Hayashi, M. Tanaka, J.B. Moffat, Surface and Bulk Properties of Stoichiometric and Nonstoichiometric Strontium Hydroxyapatite and the Oxidation of Methane, Journal of Solid State Chemistry, 126 (1996) 242-252.
[28] C. Boucetta, M. Kacimi, A. Ensuque, J.-Y. Piquemal, F. Bozon-Verduraz, M. Ziyad, Oxidative dehydrogenation of propane over chromium-loaded calcium-hydroxyapatite, Applied Catalysis A: General, 356 (2009) 201-210.
[29] J.H. Park, D.-W. Lee, S.-W. Im, Y.H. Lee, D.-J. Suh, K.-W. Jun, K.-Y. Lee, Oxidative coupling of methane using non-stoichiometric lead hydroxyapatite catalyst mixtures, Fuel, 94 (2012) 433-439.
[30] S.C. Oh, Y. Wu, D.T. Tran, I.C. Lee, Y. Lei, D. Liu, Influences of cation and anion substitutions on oxidative coupling of methane over hydroxyapatite catalysts, Fuel, 167 (2016) 208-217.
[31] K. El Kabouss, M. Kacimi, M. Ziyad, S. Ammar, A. Ensuque, J.-Y. Piquemal, F. Bozon-Verduraz, Cobalt speciation in cobalt oxide-apatite materials: structure-properties relationship in catalytic oxidative dehydrogenation of ethane and butan-2-ol conversion, Journal of Materials Chemistry, 16 (2006) 2453-2463.
[32] N. Takarroumt, M. Kacimi, F. Bozon-Verduraz, L.F. Liotta, M. Ziyad, Characterization and performance of the bifunctional platinum-loaded calcium-hydroxyapatite in the one-step synthesis of methyl isobutyl ketone, Journal of Molecular Catalysis A: Chemical, 377 (2013) 42-50.
[33] S. Ogo, A. Onda, Y. Iwasa, K. Hara, A. Fukuoka, K. Yanagisawa, 1-Butanol synthesis from ethanol over strontium phosphate hydroxyapatite catalysts with various Sr/P ratios, Journal of Catalysis, 296 (2012) 24-30.
[34] D. Chlala, M. Labaki, J.-M. Giraudon, O. Gardoll, A. Denicourt-Nowicki, A. Roucoux, J.-F. Lamonier, Toluene total oxidation over Pd and Au nanoparticles supported on hydroxyapatite, Comptes Rendus Chimie, 19 (2016) 525-537.
[35] Z. Qu, Y. Sun, D. Chen, Y. Wang, Possible sites of copper located on hydroxyapatite structure and the identification of active sites for formaldehyde oxidation, Journal of Molecular Catalysis A: Chemical, 393 (2014) 182-190.
[36] Z. Boukha, J. González-Prior, B.d. Rivas, J.R. González-Velasco, R. López-Fonseca, J.I. Gutiérrez-Ortiz, Synthesis, characterisation and behaviour of Co/hydroxyapatite catalysts in the oxidation of 1,2-dichloroethane, Applied Catalysis B: Environmental, 190 (2016) 125-136.
[37] Z. Opre, J.D. Grunwaldt, M. Maciejewski, D. Ferri, T. Mallat, A. Baiker, Promoted Ru–hydroxyapatite: designed structure for the fast and highly selective oxidation of alcohols with oxygen, Journal of Catalysis, 230 (2005) 406-419.
[38] Z. Opre, D. Ferri, F. Krumeich, T. Mallat, A. Baiker, Aerobic oxidation of alcohols by organically modified ruthenium hydroxyapatite, Journal of Catalysis, 241 (2006) 287-295.

[39] K. Zhao, B. Qiao, J. Wang, Y. Zhang, T. Zhang, A highly active and sintering-resistant Au/FeOx-hydroxyapatite catalyst for CO oxidation, Chemical Communications, 47 (2011) 1779-1781.
[40] J.H. Jun, T.-J. Lee, T.H. Lim, S.-W. Nam, S.-A. Hong, K.J. Yoon, Nickel–calcium phosphate/hydroxyapatite catalysts for partial oxidation of methane to syngas: characterization and activation, Journal of Catalysis, 221 (2004) 178-190.
[41] J.H. Jun, T.H. Lim, S.-W. Nam, S.-A. Hong, K.J. Yoon, Mechanism of partial oxidation of methane over a nickel-calcium hydroxyapatite catalyst, Applied Catalysis A: General, 312 (2006) 27-34.
[42] Z. Boukha, M. Kacimi, M. Ziyad, A. Ensuque, F. Bozon-Verduraz, Comparative study of catalytic activity of Pd loaded hydroxyapatite and fluoroapatite in butan-2-ol conversion and methane oxidation, Journal of Molecular Catalysis A: Chemical, 270 (2007) 205-213.
[43] Z. Boukha, M. Kacimi, M.F.R. Pereira, J.L. Faria, J.L. Figueiredo, M. Ziyad, Methane dry reforming on Ni loaded hydroxyapatite and fluoroapatite, Applied Catalysis A: General, 317 (2007) 299-309.
[44] K.H. Kim, S.Y. Lee, K.J. Yoon, Effects of ceria in CO2 reforming of methane over Ni/calcium hydroxyapatite, Korean Journal of Chemical Engineering, 23 (2006) 356-361.
[45] M. Uota, H. Arakawa, N. Kitamura, T. Yoshimura, J. Tanaka, T. Kijima, Synthesis of High Surface Area Hydroxyapatite Nanoparticles by Mixed Surfactant-Mediated Approach, Langmuir, 21 (2005) 4724-4728.
[46] G. Gualda, S. Kasztelan, Initial Deactivation of Residue Hydrodemetallization Catalysts, Journal of Catalysis, 161 (1996) 319-337.